

FEDSM2012-72382

**TURBULENCE RADIATION INTERACTIONS IN A STATISTICALLY HOMOGENEOUS
TURBULENCE WITH APPROXIMATED COAL TYPE PARTICULATE**

Mathew Cleveland*

Lawrence Livermore National Lab.
7000 East Ave.
Livermore, CA 94550
Email: cleveland7@llnl.gov

Sourabh Apte

Department of Mechanical Engineering
Oregon State University
Corvallis, Oregon, 97331
sva@oregonstate.edu

Todd Palmer

Department of Nuclear Engineering
Oregon State University
Corvallis, Oregon 97331
palmerts@enr.oregonstate.edu

ABSTRACT

Turbulent radiation interaction (TRI) effects are associated with the differences in the time scales of the fluid dynamic equations and the radiative transfer equations. Solving on the fluid dynamic time step size produces large changes in the radiation field over the time step. We have modified the statistically homogeneous, non-premixed flame problem of Deshmukh et al. [1] to include coal-type particulate. The addition of low mass loadings of particulate minimally impacts the TRI effects. Observed differences in the TRI effects from variations in the packing fractions and Stokes numbers are difficult to analyze because of the significant effect of variations in problem initialization. The TRI effects are very sensitive to the initialization of the turbulence in the system. The TRI parameters are somewhat sensitive to the treatment of particulate temperature and the particulate optical thickness, and this effect is amplified by increased particulate loading.

INTRODUCTION

Heterogeneous transport has been extensively studied, particularly in the field of neutron transport, since the 1940's [2]. Pulverized coal combustion involves many material heterogeneities such as flue gas, coal particles, fly ash, and char. These heterogeneities can best be described as stochastic mixtures. A stochastic mixture is a combination of two or more materials that can be defined by a statistical distribution. Work by Marakis et

al. showed that wall heat fluxes are strongly affected by the presence of each of these materials [3].

Particle interactions in radiative heat transfer include four different phenomena [4]; diffraction, refraction, reflection, and absorption. There are a variety of ways to predict and account for these different phenomena, including Lorenz-Mie theory, Rayleigh theory, and geometric optics. The accuracy of each method is greatly dependent on the frequency of the photon, the particle size, and particle material properties [4].

The effects from Turbulence Radiation Interactions (TRI) in particulate laden flows can have a significant effect on thermal radiation fields and corresponding material heating [5]. Radiative heat transfer has been extensively studied in a variety of stochastic media including combustion problems [5–8]. Most combustion problems contain strong heterogeneities which can be treated stochastically. In pulverized coal combustion, these heterogeneities include particulate such as coal, fly-ash, and char [3, 5]. These materials are typically accounted for stochastically using an atomic mix model. TRI effects have been shown to be very sensitive to the presence of soot in turbulent flames, significantly decreasing mean flame temperatures [9].

Four primary methods have been employed to solve stochastic mixture problems; the brute force method, atomic mixing, chord length sampling, and lattice structures [10]. A variety of sensitivity studies have been performed by Liu [11, 12] on particle size and temperature distributions. These studies show that radiative transfer, particularly in high-temperature environments, can be significantly affected by differences in particle properties.

*Address all correspondence to this author. LLNL-CONF-549831

This work expands upon a simplified test case, developed by Deshmukh et al. [1], to highlight the effects of fuel particulate on TRI phenomena. The code used in this work is a 3D parallel coupled radiative heat transfer and reacting fluid flow solver. The radiative heat transfer equation is solved via the Monte Carlo method. Radiation interactions with particulate can be accounted for either using Mie theory [13] or geometric optics [4] depending on particulate size. The reacting fluid flow model solves the continuity equation, the compressible or incompressible Navier-Stokes equations, the mixture fraction equations, and energy equation. The compressible Navier-Stokes equations are solved using a Large-eddy simulation (LES) [14] model, and particle-fluid interactions are accounted for using Discrete Element Modeling (DEM) [14].

Particulate properties, specifically material temperatures, can be treated in a variety of ways. Small particulate such as fly-ash, char, and very small coal particulate are typically assumed to exist at the mean cell temperature. This a relatively good assumption because these materials are physically very small and dissipate any excess heat very quickly. The coal particulate can be more difficult because the relatively large size of the particulate means that it will have heat latency that should not be neglected. It is suggested that coal particulate likely remains close to the original inlet temperature and the majority of thermal emission occurs in the soot envelope that forms immediately around the particulate during combustion [15].

GOVERNING EQUATIONS

Modeling a combustion system requires the solution of a set of coupled non-linear equations. These equations include; the continuity equation, the compressible/incompressible Navier-Stokes equations, mixture fraction equations, the radiative transfer equation, and the energy equation. Each of these equations presents its own solution challenges, combining these difficulties with significant differences in time scale makes these problems very difficult to solve efficiently and accurately. This work focus on the efficient implementation of the time-integrated radiative transfer equation which has been decoupled from the fluid flow.

The time dependent radiative transfer equation can be written as;

$$\frac{1}{c} \frac{dI}{dt} + \bar{\Omega} \cdot \bar{\nabla} I + KI = \frac{K}{4\pi} B \quad (1)$$

where the independent variables have been left out for brevity. Here $I(\bar{r}, \bar{\Omega}, \nu, t)$ [ergs/sec-cm²-steradians-Hz] is the radiative intensity as a function of position (\bar{r}) [cm], solid angle ($\bar{\Omega}$) [steradians], frequency (ν) [Hz], and time (t) [sec], $K(\nu, \bar{r})$ [1/cm] is the opacity, c [cm/sec] is the speed of light, and $B(\nu, T)$ is the Planck function.

The material energy balance equation is written as

$$\frac{dq_R}{dt} = \int_0^\infty \int_0^{4\pi} KI d\bar{\Omega} d\nu - \int_0^\infty \int_0^{4\pi} \frac{K}{4\pi} B d\bar{\Omega} d\nu, \quad (2)$$

where q_R is the material energy density.

The mixture fraction equation can be written as;

$$\rho \left(\frac{dY_i}{dt} + \bar{U} \cdot \bar{\nabla} Y_i \right) = \bar{\nabla} \cdot \rho D \bar{\nabla} Y_i + \dot{m}_i''' \quad (3)$$

The mass source (\dot{m}_i''') and the heat source ($\dot{Q}_c''' h$) are products of the chemical reaction;



In this reaction O , F , and P denote the concentration of oxidizer, fuel, and the resulting product P . The variable Q represents the amount of energy released during the reaction.

PARTICULATE

The inclusion of particulate in the system requires the addition of a model to account for fluid-particulate interactions. In this research, we use the discrete element model (DEM) [14] to account for these two-way interactions. An important parameter to classify the state of the particulate-laden flow is the Stokes number. The Stokes number is a ratio of the particulate response time (τ_p) to the Kolmogorov time scale (τ_η) [16];

$$St = \frac{\tau_p}{\tau_\eta} = \frac{1}{18} \left(\frac{\rho_p}{\rho} \right) \left(\frac{d_p}{\eta} \right)^2 \quad (5)$$

The variables ρ and ρ_p are the fluid and particulate density, respectively. The remaining variables are the particulate diameter d_p and Kolmogorov length scale η . It is known that when $St \approx 1$ “preferential concentrations” occur. This is when the local vorticity is strong enough to force particulate out of fluid regions causing particulate clustering [16]. This is important to radiative transfer because it affects particle dispersal and the accuracy of the chord length method, which makes assumptions about the distribution of particulate in background media.

It is also necessary to account for particulate-radiation interactions. Particulate-radiation interactions can either be accounted for using Mei theory or geometric optics, depending on the particulate size parameter and optical thickness. Our focus is on larger coal particulate, where geometric optics is valid. All particulate in this work is considered to be perfect spheres.

The interaction of radiation with particulate is very sensitive to the size, shape, and material composition of the particulate. For large particulate, diffraction can be neglected allowing for the evaluation of particulate interactions using geometric optics [4]. Large particulate is quantified as $x \gg 1$, where x is the non-dimensional size parameter defined by;

$$x = \frac{\pi D_p}{\lambda} > 2, \quad (6)$$

and D_p is the diameter of the particulate and λ is the photon wavelength. If $x \approx 1$ then diffraction can no longer be neglected and Mie theory is applied to determine interaction probabilities.

There are four different particulate-radiation interactions that must be considered: reflection, refraction, diffraction, and absorption. For large thick particulate, diffraction and refraction can be neglected because for large particles diffraction generally scatters in the forward direction [4]. For smaller particulate, however, diffraction can become more isotropic and must be modeled [4]. Diffraction is generally modeled using Mie theory [4]. If the particulate is reasonably optically thick ($xk \gg 1$) all photons that enter the particulate are assumed to be absorbed, and refraction events can be neglected. However, for optically thin particulate, this assumption is not valid.

For geometric optics, the probability of a ray intersecting a particulate can be evaluated: stochastically or geometrically using direct tracking. Stochastic methods include atomic mixing and the chord length method [17]. Direct tracking simply includes the particulate either directly in the mesh or on a submesh which is overlaid on the cell mesh. The implementation of the chord length methods used in this work has been previously discussed in detail by Cleveland [18]

TURBULENCE RADIATION INTERACTIONS

The significant difference in time scales for the radiative transfer equation and the turbulent flow equation can create a unique numerical phenomenon known as Turbulence Radiation Interactions (TRI). The time scale of the flow equations is on the order of the speed of sound for the working fluid whereas the time scale of the radiation equation is on the order of the speed of light. Comparing the temporal operator of the transport equation to that of the fluid equations, we find that unless the time step size is on the order of the speed of light, the transport equation will quickly approach the steady state solution. If the equations are evaluated over a conventional fluid time step (some reasonable fraction of the speed of sound) a certain amount of material fluctuation will occur in cells that are turbulent or not fully developed. These material fluctuations will be felt instantaneously, locally and globally, by the radiative transfer equations. Though it is possible to resolve these numerical differences by resolving the

material fluctuations on the order of the radiative transfer equation, for most real applications is prohibitively computationally expensive. To account for these interactions, the equations are typically rewritten and solved for time averaged quantities [4].

$$\overline{f(r)} = \frac{1}{\delta t} \int_{\delta t} f(r,t) dt \quad (7)$$

The transport equation is written in the time-averaged form as;

$$\frac{1}{c\delta t} (I_{n+1} - I_n) + \bar{\Omega} \cdot \bar{\nabla} \bar{I} + \bar{K} \bar{I} = \frac{1}{4\pi} \bar{K} \bar{B}, \quad (8)$$

and the equation of state becomes

$$\frac{dq_R}{dt} = \int_0^\infty \int_0^{4\pi} \bar{K} \bar{I} d\bar{\Omega} dv - \int_0^\infty \int_0^{4\pi} \frac{1}{4\pi} \bar{K} \bar{B} d\bar{\Omega} dv. \quad (9)$$

Evaluating these time-averaged quantities requires at least one more assumption, known as the optically thin eddy approximation. The optically thin eddy approximation assumes that the time averaged opacity multiplied by the time averaged intensity is equivalent to the time averaged absorption operator ($\overline{\bar{K} \bar{I}} \approx \bar{K} \bar{I}$) [4]. This implies that the opacity multiplied by the turbulence length scale is small ($K l_t \ll 1$). This condition is typically violated in some frequency regions for gas opacities. However, this assumption has been made in all TRI work to date [4].

There are commonly four different approaches to deal with TRI effects [4]. Using the time averaged material properties to evaluate the radiation field, referred to as ‘‘no TRI’’, implies

$$\bar{K}_v = K_v(\bar{\phi}); \quad \overline{K_v b(v, T)} = K_v(\bar{\phi}) b(v, \bar{T}). \quad (10)$$

Where $b(v, \bar{T})$ is the normalized Planck function.

The variable $\bar{\phi}$ refers to the time averaged material state. The next approach attempts to account for the non-linear correlation between the material properties and the opacity by using the mean opacity rather than the mean material properties. This is commonly referred to as ‘‘absorption coefficient self-correlation’’,

$$\bar{K}_v; \quad \overline{K_v b(v, T)} = \bar{K}_v b(v, \bar{T}). \quad (11)$$

It is also possible to account for the non-linearities of the opacity values and the Planck emission spectrum using ‘‘Planck function self-correlation’’

$$\bar{K}_v; \quad \overline{K_v b(v, T)} = K_v(\bar{\phi}) \overline{b(v, T)}. \quad (12)$$

Finally, it is possible to combine the absorption coefficient and Planck function self-correlations. This is referred to as “full TRI”, even though this approach is still approximate as a result of the optically thin eddy approximation:

$$\overline{K_v}; \quad \overline{K_v b(v, T)}. \quad (13)$$

It is obvious that there is non-linear feedback between the radiation field and the material properties. This correlation is generally neglected because of the computational cost of evaluating both the radiative transfer equations and the turbulent flow. Treating the material fluctuations as a separate uncorrelated event from the radiative transfer equation allows for the development of material fluctuation probabilities for the individual cells. These material fluctuation models can be used to directly evaluate the time averaged emission source and cell opacities (full TRI).

A statistically homogeneous, turbulent, idealized, gas combustion flame is modeled in this work, as described by [1], such that every cell in the domain represents a single probable state of the material at that instant in time. In this simplified test case, the radiative transfer equation is not coupled to the material energy balance equation and all material properties are directly related to the combustion product concentration. As a result, the material properties are directly determined from the gas combustion process, circumventing the need to resolve the nonlinearities between the equations. These approximations allow for the creation of a combustion simulation capability that provides insightful quantitative results to analyze the impact of the TRI phenomenon.

The main TRI parameters that will be investigated in this work are the following three normalized means;

$$R_{T^4} = \frac{\overline{T^4}}{\overline{T}^4}, \quad (14)$$

$$R_{K I_b} = \frac{\overline{K_p I'_b}}{\overline{K_p} \overline{I_b}}, \quad (15)$$

and

$$R_{K G} = \frac{\overline{K' G'}}{\overline{K} \overline{G}}. \quad (16)$$

These means demonstrate the errors associated with using the mean material properties, the Planck self-correlation, and the thin eddy approximation (Equations 14, 15, and 16 respectively).

TRI run cases			
Test Case ID	Stokes #	$\tilde{\rho}_p$ [kg/m ³]	Packing fraction
TRI_1	0.0	0.0	0.0
TRI_4	2.3	900	9.6e-2 %
TRI_5	2.3	900	1.9e-1 %

TABLE 1. VARIATIONS OF THE TRI TEST PROBLEM

Consistent Run Parameters		
Parameter	Value	Units
Reynolds #	77	N/A
Prandtl #	0.75	N/A
Lewis #	1.0	N/A
Fluid Density	1.0	kg/m ³
Particle Diameter	0.012	m
T_min	750	K
T_max	3000	K

TABLE 2. FLOW SOLVER RUN PARAMETERS USED FOR ALL TEST CASES

The primed coefficients represent the difference in the true average from the approximate average;

$$K' G' = \overline{K G} - \overline{K} \overline{G}. \quad (17)$$

and G is the scalar radiative intensity ($G = \int_0^{4\pi} I d\bar{\Omega}$).

TEST CASE

In the test problem developed by Deshmukh et al., a fully periodic three dimensional domain is defined. A velocity forcing function [19] initiates statistically homogeneous turbulence in the system. Three different variations of the Deshmukh problem were considered: one without particulate and two different particulate-laden problems using various Stokes numbers and different packing fractions. Specific details of these problems can be found in Tables 1 and 2.

All particulate simulations were started from the same initial restart problem. The turbulent kinetic energy (Eq. 18) was monitored to verify that the problem had reached a statistically steady state flow pattern. Figures 1, and 2 show particulate distributions

in a thin slice (1/64 of the total length) of the domain. In these figures, the dots indicate the particulate center locations. The variable $Npar$ in the title of Figure 2 refers to the number of particulate spheres represented by each point; in this case one point is representative of two particulate spheres. A larger $Npar$ allows for a reduction in computational resources while still being able to account for larger packing fractions. After the system reaches a statistically steady state flow regime, as determined from the fluctuations in the turbulent kinetic energy;

$$\frac{\partial \langle \bar{u} \cdot \bar{u} \rangle}{\partial t} \approx 0. \quad (18)$$

the simulation is paused and populated randomly with fuel and oxidizer via the approach described by Eswaran et al. [20]. This initialization relies on the use of a Fourier transform in which the Fourier amplitudes are randomly selected and then inversely transformed back to physical space and used to populate the material properties. This helps smooth the random double- δ distribution in space. [Every cell is either pure fuel or oxidizer.] This defines the initial material distribution in a manner consistent with Deshmukh et al. [1]. Our research does not use the wavenumber filter originally described in the Eswaran [20] paper. This results in a significantly faster build-up of combustion products. Figures 3 and 4 are example slices of the fuel concentration after the first time step and the final time step of a single TRI simulation. These plots show that after the first time step a significant amount of the fuel has reacted with the oxidizer and at the final time step nearly all of the fuel has reacted.

PARTICULATE PROPERTIES

The material properties for the particulate are chosen to represent properties that would be expected in pulverized coal combustion systems. There are three main classifications of coal; anthracite (greater than 86% fixed carbon, less than 14% volatile matter), bituminous (greater than 86% fixed carbon, less than 14% volatile matter, greater than 10,500 Btu), and lignite (less than 8,300 Btu) [21]. Each of these classifications reflect generalized composition and potential energy parameters. We have chosen bituminous coal properties in this research.

Manickavasagam et al. [22] found that the refraction index n in a specific type of bituminous coal, Kentucky coal #9, was relatively insensitive to photon frequency. This has been found in other published literature [4, 22]. Given the definition of the material opacity, K is proportional to the absorptive index and the photon frequency. It is possible to develop an approximate opacity that is independent of frequency by fitting the absorptive index, as a function of frequency, with a linear function that is

inversely proportional to the frequency: $k \approx k_f = \frac{k_0}{\nu}$.

$$K = \frac{4\pi k \nu}{c_0} = \frac{4\pi k_0}{c_0} \quad (19)$$

We have used a least-squares fit of the polynomial representation of the bituminous coal (Kentucky coal #9) absorptive index provided by Manickavasagam et al. [22]. A graphical representation of the fit can be found in Figure 5. The least-squares fit was found such that the derivative of the sum of the square of the relative errors is zero;

$$R^2 = \sum_{i=1}^N (k(\nu_i) - k_f(\nu_i))^2 \quad (20)$$

$$\frac{dR^2}{dk_f} = 0 = 2.0 \sum_{i=1}^N (k(\nu_i) - k_f(\nu_i)) \frac{1}{\nu_i} \quad (21)$$

This sum can be directly evaluated and solved for k_0 ;

$$k_0 = \sum_{i=1}^N \frac{k(\nu_i)}{\frac{1}{\nu_i^2}} \quad (22)$$

using 100 data points in the wavelength range $3 \leq \lambda \leq 19$ [μm] results in a fitted coefficient of $k_0 = 1.4806e - 2$ [$\frac{1}{\mu m}$].

The Stokes number as defined in Equation 5 indicates the amount of particulate clustering in the system. This equation can be used to determine an effective particulate density that will yield a desired Stokes number, given the particulate properties, the fluid properties, and the Kolmogorov length scale indicative of the fluid flow profile:

$$\tilde{\rho}_p = 18St\rho_f \left(\frac{\eta}{d_p} \right)^2 \quad (23)$$

Both the fluid field and the radiation field are directly proportional to the particle diameter as indicated by Equations 5 and 6, respectively. In order to keep the radiation field insensitive to the fluid flow, (as in the work of Deshmukh et al. [1]), the radiation properties of the coal are scaled such that they match properties typically found in pulverized coal systems. The bulk of coal particulate found in pulverized coal is on the scale of $d_p = 5.8$ [μm] [22]. Note that this is not the bulk from a mass perspective, but rather from the perspective of the total number of particles. In this work, all particulate is assumed to be of equal size. Using

this particulate size and the fitted gray opacity value K , it is possible to determine the effective opacity \tilde{K} such that the diameter in number of mean free paths is equivalent $\frac{d_p}{M_{fp}} = \frac{\tilde{d}_p}{M_{fp}}$. A mean free path is defined as;

$$M_{fp} = 1/K, \quad (24)$$

and the particle diameter as a function of mean free paths can be defined as;

$$N_{mfp} = \frac{d_p}{M_{fp}}. \quad (25)$$

Given these definitions the effective opacity can be evaluated as;

$$\tilde{K}_p = \frac{N_{mfp}}{\tilde{d}_p} \quad (26)$$

NUMERICAL RESULTS

The mixture fraction is the driving parameter in these simulations because it determines all material properties. This completely drives the radiation solution. Figure 6 shows the variance of the mixture fraction as a function of non-dimensional time for the different problem initializations presented in Table 1.

There are two common ways to treat the particulate temperature: constant, equal to the initial temperature, or equal to the mean cell temperature in which it resides. Fly ash and char are typically treated at the mean cell temperature because of their size. Coal particulate on the other hand is considerably larger and therefore is less sensitive to the cell temperature. The difference in the normalized mean of the temperature (Equation 14) is shown in Figure 7.

Figure 8 shows the normalized temperature mean (R_T^4) for all three different cases. In all the cases shown in this figure, the mean cell temperature was used for the temperature of the particulate. Variations in these curves are strongly correlated to the variations in the mixture fraction (Figure 6).

The normalized emission mean (Equation 15) is also strongly driven by variations in the mixture fraction and particulate opacity. Figure 9 shows the difference in the means when using a constant particulate temperature versus the cell mean temperature.

The normalized emission mean (R_{KI_b}) depends on the temperature treatment of the particulate, and the opacity. To assess the sensitivity, three different opacity values were chosen ($K_p = 9.2, K_p = 92, \text{ and } K_p = 920$). Figure 10 shows the difference in the normalized emission mean for the three different opacities with $St=2.3$ and $Npar=1$.

Figure 11 shows all the normalized emission mean values for the various problem initializations outlined in Table 1. The differences in these curves correlate with the differences in the material mixture fraction variance, shown in Figure 6.

The normalized absorption mean (Equation 16) is strongly dependent on both the radiation source term and opacity distribution. The statistical noise in this quantity make it difficult to evaluate. Changes can best be illustrated by comparing the normalized means of the cases that should have the greatest differences. The problem is most sensitive to the mixture variance. The second most sensitive variable is the particulate thickness. Figure 12 shows the normalized absorption mean (R_{KG}) for the test case without particulate and the test case with $St=2.3, Npar = 1, K_p = 920$, and the particulate temperature defined as the cell mean temperature. These cases should have the greatest difference because of the sensitivity to mixture variance and particulate thickness.

To observe the effect of particulate thickness, Figure 13 shows the thin test problem ($K_p = 9.2$) and the thick test problem ($K_p = 920$). Figure 14 shows the dependence on the particulate temperature definition using the $St=2.3$ and $Npar = 2$ test case.

CONCLUSIONS

Deshmukh et al. [1] developed a numerical test case that could be used to evaluate the sensitivity of turbulent radiation interactions to a variety of parameters. We have expanded upon this test case to determine the sensitivity of TRI to the addition of coal-type particulate. Other particulate, such as fly ash and char, have been extensively studied and have been shown to strongly affect mean flame temperatures and radiative heat fluxes [3,9].

Coal particulate is more sensitive to flow regimes than smaller particulate, such as fly ash and char, because of its relative size and momentum. To evaluate the effect of the presence of coal particulate on overall TRI, two simulations with different Stokes numbers were performed ($St=2.3$ and $St=0.0$). Because the particulate density will also vary in combustion applications, two packing fractions were considered ($9.6e-2\%$ and $1.9e-1\%$). The initial particle clustering in each of these simulations is evident in Figures 1 and 2. These figures show thin slices of the spatial domain, and every dot represents a single particle location, with the exception of Figure 2, where every dot represents two particulate spheres. At low Stokes numbers, clustering begins to occur and as the Stokes number is increased beyond 1, collisions begin to push the particulate back into the eddies which originally pushed them out.

Because the smoothing filter was not applied to the initialization of the material distribution, the rate of product build-up is much faster than in the work of Deshmukh et al. [1]. This is evident from a plot of the fuel distribution after one time step (Figure 3). In fact, the fuel is almost completely combusted after the non-dimensional time of 0.05 (see Figure 4). The mixture frac-

tion is the driving parameter for the radiative transfer equations in this problem. Figure 6 shows a slightly different progression of the mixture variance as a function of time for each of the initializations. This likely relates directly to the initial kinetic energy in the system before it is populated with fuel, and before the turbulence is allowed to decay. The differences in the decay rates of the mixture variance are observed in two of the normalized TRI means (Figures 8 and 11). This is by far the most influential parameter in the system. Therefore, any variations associated with varying Stokes numbers and packing fractions are difficult to discern from a direct comparison.

To illustrate the influence of the definition of the particulate temperature, each simulation was performed once using a constant particulate temperature (of 750[K]) and once assuming the particulate temperature is equal to the mean background medium cell temperature. Figure 7 compares the normalized temperature mean (R_{T^a}) for the two different definitions of the particulate temperature. These figures show that the TRI normalized temperature mean is relatively insensitive to the particulate temperature definition. The evolution of the packing fraction is most sensitive to the definition of the particulate temperature. It is expected that as the number density and/or size of the particulate is increased, the problem will become increasingly more sensitive to the definition of particulate temperature. This is because larger and/or more clustered particulate will likely maintain lower temperatures, increasing TRI effects. Figure 9 shows the normalized emission mean (R_{Klb}) for all three particulate initializations with both the constant particulate temperature and mean cell particulate temperatures. This mean is even less sensitive to the definition of the particulate temperature.

Figure 10 shows the dependence of the normalized emission mean on the particulate optical thickness. This figure shows that as the particulate becomes more optically thick, the TRI effects associated with the emission term decrease. As the influence of the particulate becomes more prominent, its smoother (in this case constant) opacity means that the emission source distribution will be more consistent throughout the problem.

Statistical variance in the normalized absorption mean (R_{KG}) makes it very difficult to quantify the effect of parameter variations. Therefore, only the simulations which should have the most significant differences (as determined by the differences in the other means) are plotted. The two most significant differences associated with the other means are the rate of reduction in mixture variance and particulate optical thickness. Figure 12 compares the normalized absorption means for the two cases that are the most different in opacity and mixture variance. Even in these cases, it is difficult to draw any conclusions about the differences in the results because of the significant statistical noise in the solutions. Figures 13 and 14, comparing the differences associated with particulate thickness and temperature treatment, show some discernible differences. Making the problem thicker or treating the particulate as a constant temperature appears to

reduce the statistical noise. This does show that the influence of the particulate on the optically thin eddy approximation is relatively mild. Even for the thickest particulate, the overall maxima and minima of the curves remain relatively unaffected.

This work shows that TRI effects are relatively insensitive to non-combusting coal-type particulate for low mass loadings. The least sensitive TRI parameter is the normalized absorption mean (or optically thin eddy approximation). As mass loading increases and coal combustion processes are included, the TRI effects will likely be amplified. This is because the source term in the radiative transfer equation will be tightly coupled to the location and density of the particulate.

A great deal of care was taken in this work to preserve the physical properties of a coal combustion problem with low packing fractions. However, larger packing fractions should also be compared to gain more insight into TRI effects associated with heavily particulate laden zones (i.e. near fuel inlets). It would also be beneficial to perform some simulations in which the radiation source is driven by the particulate rather than the gas. This would be more representative of a real combustion process for pulverized coal. These simulations are left for future work.

ACKNOWLEDGEMENTS

This work was supported by Department of Energy-National Energy Technology Laboratory under URS Contract No. 41817M4077. We wish to thank Dr. Cathy Summers (NETL, Albany) for monitoring this work.

This work performed under the auspices of the U.S. Department of Energy by Lawrence Livermore National Laboratory under Contract DE-AC52-07NA27344.

REFERENCES

- [1] Deshmukh, K., Haworth, D., and Modest, M., 2007. "Direct numerical simulation of turbulence-radiation interactions in homogeneous nonpremixed combustion systems". *Proceedings of the Combustion Institute*, **31**(1), Jan., pp. 1641–1648.
- [2] Duderstadt, J. J., and Hamilton, L. J., 1976. *Nuclear reactor analysis*.
- [3] Marakis, J. G., Papapavlou, C., and Kakaras, E., 2000. "A parametric study of radiative heat transfer in pulverised coal furnaces". *International Journal of Heat and Mass Transfer*, **43**(16), Aug., pp. 2961–2971.
- [4] Modest, M. F., 2003. *Radiative heat transfer*. Academic Press.
- [5] Haworth, D., 2010. "Progress in probability density function methods for turbulent reacting flows". *Progress in Energy and Combustion Science*, **36**(2), Apr., pp. 168–259.
- [6] Olson, G. L., Miller, D. S., Larsen, E. W., and Morel, J. E., 2006. "Chord length distributions in binary stochastic me-

- dia in two and three dimensions”. *Journal of Quantitative Spectroscopy and Radiative Transfer*, **101**(2), Sept., pp. 269–283.
- [7] Miller, D. S., Graziani, F., and Rodrigue, G., 2001. “Benchmarks and models for time-dependent grey radiation transport with material temperature in binary stochastic media”. *Journal of Quantitative Spectroscopy and Radiative Transfer*, **70**(1), July, pp. 115–128.
- [8] Wang, A., Modest, M. F., Haworth, D. C., and Wang, L., 2008. “Monte carlo simulation of radiative heat transfer and turbulence interactions in methane/air jet flames”. *Journal of Quantitative Spectroscopy and Radiative Transfer*, **109**(2), Jan., pp. 269–279.
- [9] Tess, L., Dupoirieux, F., and Taine, J., 2004. “Monte carlo modeling of radiative transfer in a turbulent sooty flame”. *International Journal of Heat and Mass Transfer*, **47**(3), Jan., pp. 555–572.
- [10] Reinert, D. R., 2008. “Investigation of stochastic radiation transport methods in random heterogeneous mixtures”.
- [11] Liu, L., 2003. “A concept of multi-scale modeling for radiative heat transfer in particle polydispersions”. *Journal of Quantitative Spectroscopy and Radiative Transfer*, **78**(2), May, pp. 227–233.
- [12] Liu, L., 2003. “Multiple size group analysis for transient radiative heating of particle polydispersions”. *Journal of Quantitative Spectroscopy and Radiative Transfer*, **76**(2), Jan., pp. 225–234.
- [13] Hulst, H. C., 1981. *Light scattering by small particles*. Courier Dover Publications.
- [14] Apte, S., Mahesh, K., Moin, P., and Oefelein, J., 2003. “Large-eddy simulation of swirling particle-laden flows in a coaxial-jet combustor”. *International Journal of Multiphase Flow*, **29**(8), Aug., pp. 1311–1331.
- [15] Bejarano, P. A., and Levendis, Y. A., 2008. “Single-coal-particle combustion in O₂/N₂ and O₂/CO₂ environments”. *Combustion and Flame*, **153**(1-2), Apr., pp. 270–287.
- [16] Reade, W. C., and Collins, L. R., 2000. “Effect of preferential concentration on turbulent collision rates.”. *Physics of Fluids*, **12**(10), Oct., p. 2530.
- [17] Donovan, T., and Danon, Y., 2003. “Application of monte carlo Chord-Length sampling algorithms to transport through a Two-Dimensional binary stochastic mixture”. *Nuclear Science and Engineering*, **143**(3), pp. 226–239.
- [18] Cleveland, M. A., 2011. Radiative heat transfer in combustion applications : parallel efficiencies of two gas models, turbulent radiation interactions in particulate laden flows, and coarse mesh finite difference acceleration for improved temporal accuracy. <http://scholarsarchive.library.oregonstate.edu/xmlui/handle/1957/26119>, Dec. Graduation date: 2012.
- [19] Lundgren, B. T. S., 2003. “Linearly forced isotropic turbulence”. *Center for Turbulence Research*, **2**, pp. 461–473.
- [20] Eswaran, V., and Pope, S. B., 1988. “Direct numerical simulations of the turbulent mixing of a passive scalar”. *Physics of Fluids*, **31**(3), p. 506.
- [21] Wood, G., Kehn, T., Carter, M. D., and Culbertson, W., 2003. Circular 891 - glossary of coal classification system and supplementary terms. Tech. rep., USGS.
- [22] Manickavasagam, S., and Menguc, M. P., 1993. “Effective optical properties of pulverized coal particles determined from FT-IR spectrometer experiments”. *Energy & Fuels*, **7**(6), Nov., pp. 860–869.

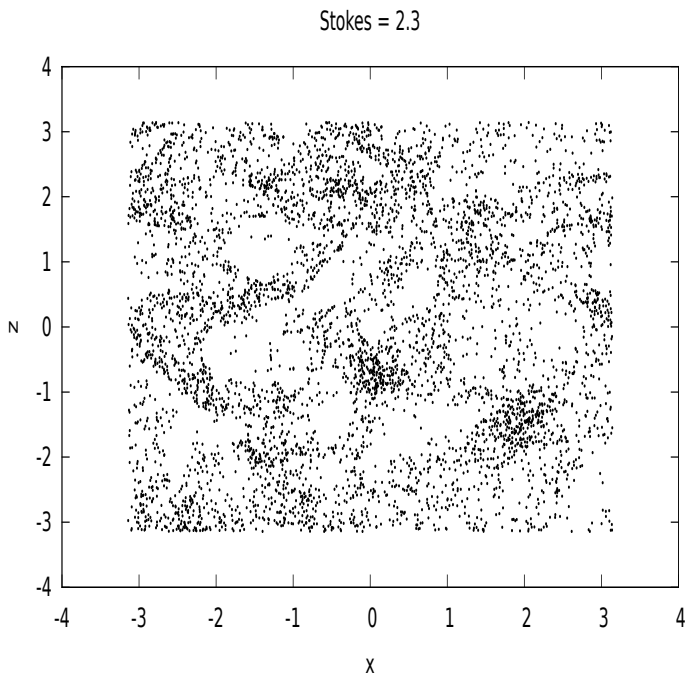


FIGURE 1. PARTICULATE CLUSTERING FOR A STOKES NUMBER OF 2.3

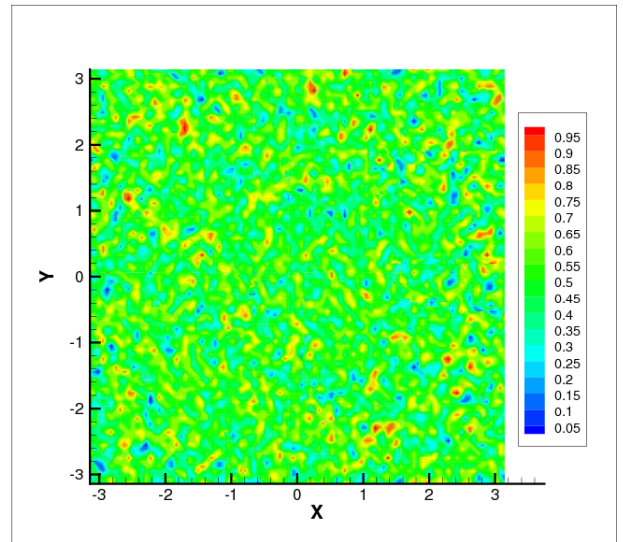


FIGURE 3. FUEL CONCENTRATION AFTER A SINGLE TIME STEP

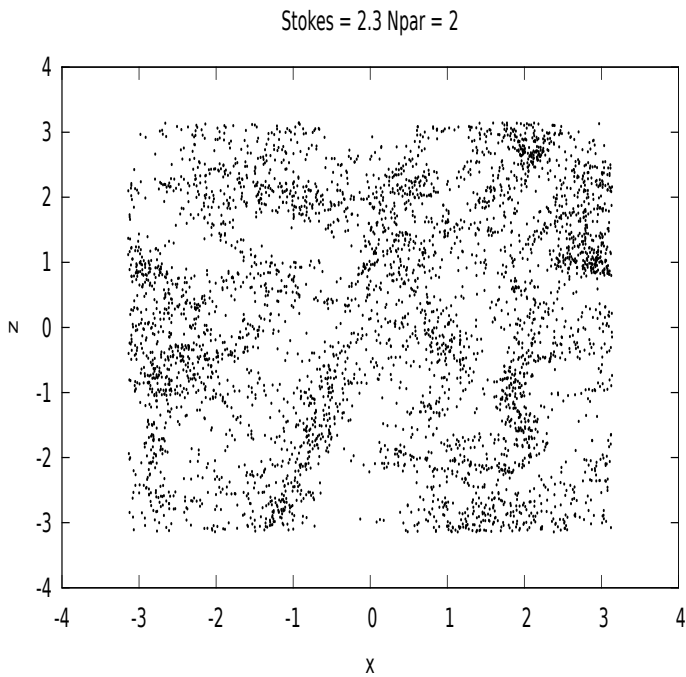


FIGURE 2. PARTICULATE CLUSTERING FOR A STOKES NUMBER OF 2.3 AT TWICE THE PACKING FRACTION USED IN FIGURE 1

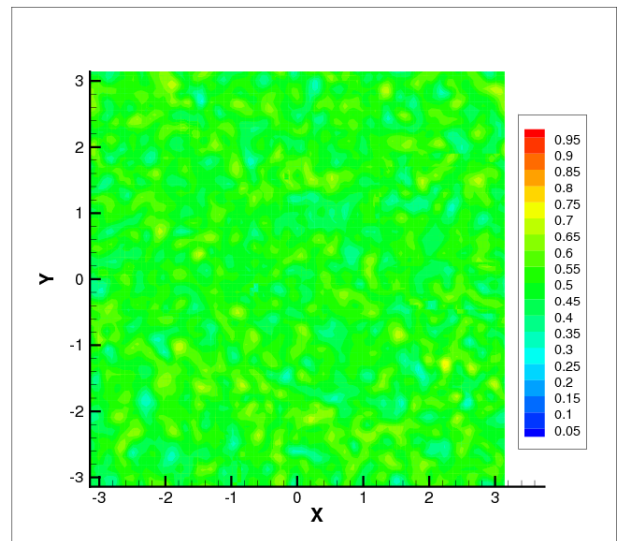


FIGURE 4. FUEL CONCENTRATION AFTER THE FINAL TIME STEP

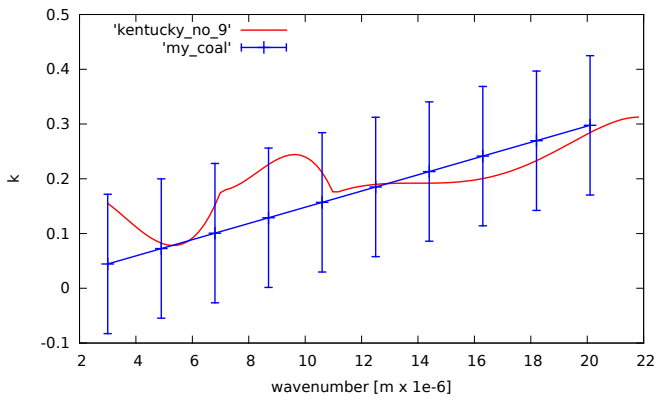


FIGURE 5. LEAST-SQUARES FIT PROVIDED BY MANICKAVASAGAM ET AL. [22]

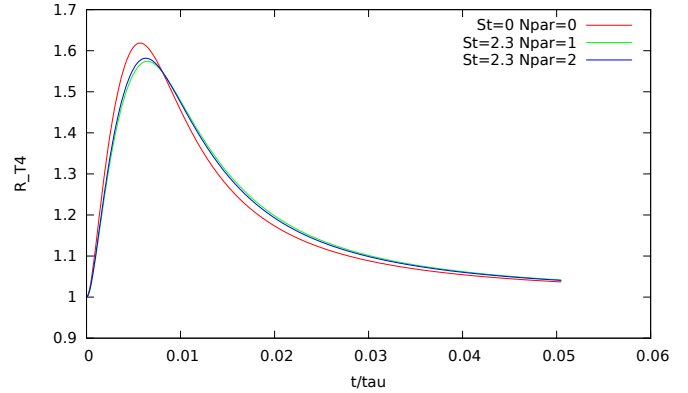


FIGURE 8. THE NORMALIZED TEMPERATURE MEANS (R_{T4}) FOR THE THREE DIFFERENT PROBLEM INITIALIZATIONS OUTLINED IN TABLE 1

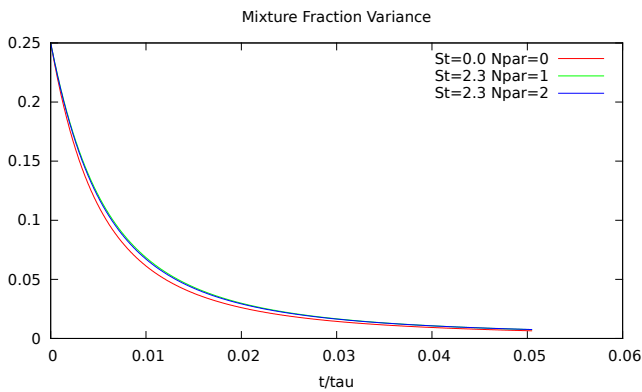


FIGURE 6. VARIANCE OF THE MIXTURE FRACTION FOR THE DIFFERENT RUN PARAMETERS

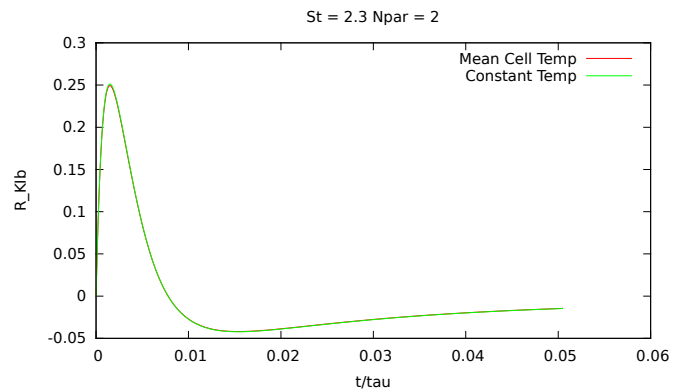


FIGURE 9. CONSTANT TEMPERATURE VERSUS MEAN CELL TEMPERATURE TREATMENTS FOR $St=2.3$ WITH TWICE THE PACKING FRACTION ($Npar = 2$)

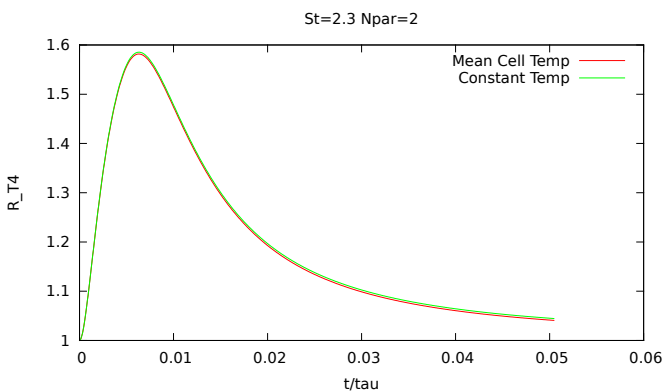


FIGURE 7. CONSTANT TEMPERATURE VERSUS MEAN CELL TEMPERATURE TREATMENTS FOR $St=2.3$ WITH TWICE THE PACKING FRACTION ($Npar = 2$)

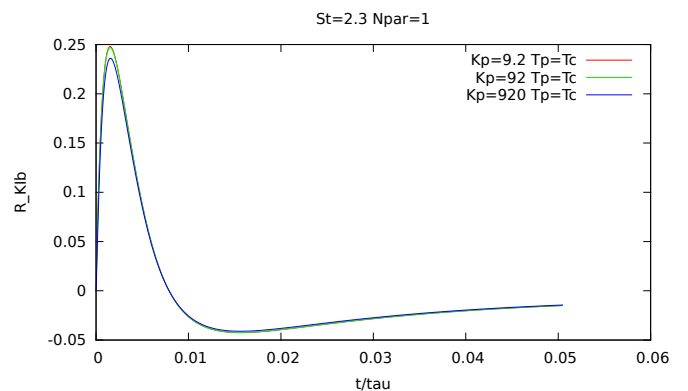


FIGURE 10. CONSTANT TEMPERATURE VERSUS MEAN CELL TEMPERATURE TREATMENTS FOR $St=2.3$ WITH TWICE THE PACKING FRACTION ($Npar=2$)

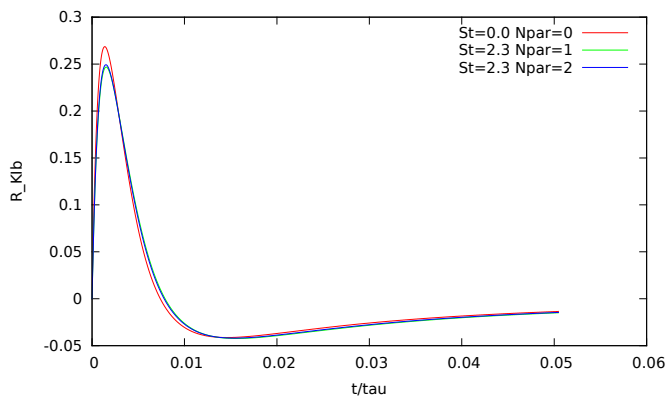


FIGURE 11. NORMALIZED EMISSION MEANS FOR ALL THREE DIFFERENT CASES.

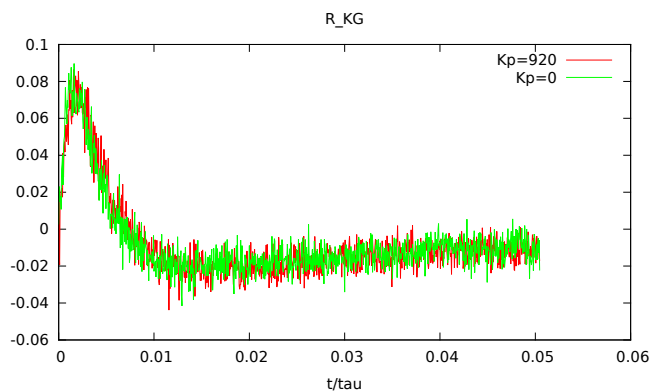


FIGURE 12. NORMALIZED ABSORPTION MEANS FOR THE CASES WITH THE GREATEST DIFFERENCE IN OTHER MEANS

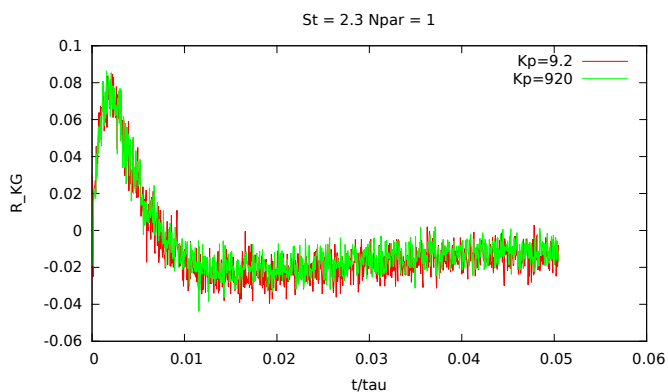


FIGURE 13. NORMALIZED ABSORPTION MEANS FOR THICK VERSUS THIN PARTICULATE

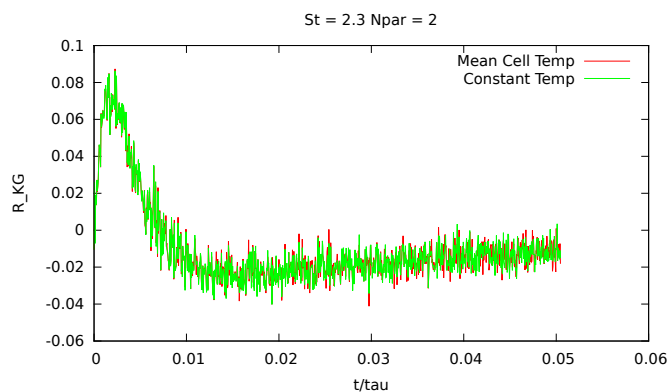


FIGURE 14. NORMALIZED ABSORPTION MEAN FOR CONSTANT PARTICULATE TEMPERATURE VERSUS PARTICULATE TEMPERATURES AT THE MEAN CELL TEMPERATURE